

Simultaneous measurement of forward-backward asymmetry and top polarization in dilepton final states from $t\bar{t}$ production at the Tevatron

V. M. Abazov,³¹ B. Abbott,⁶⁷ B. S. Acharya,²⁵ M. Adams,⁴⁶ T. Adams,⁴⁴ J. P. Agnew,⁴¹ G. D. Alexeev,³¹ G. Alkhazov,³⁵ A. Alton,^{56a} A. Askew,⁴⁴ S. Atkins,⁵⁴ K. Augsten,⁷ C. Avila,⁵ F. Badaud,¹⁰ L. Bagby,⁴⁵ B. Baldin,⁴⁵ D. V. Bandurin,⁷³ S. Banerjee,²⁵ E. Barberis,⁵⁵ P. Baringer,⁵³ J. F. Bartlett,⁴⁵ U. Bassler,¹⁵ V. Bazterra,⁴⁶ A. Bean,⁵³ M. Begalli,² L. Bellantoni,⁴⁵ S. B. Beri,²³ G. Bernardi,¹⁴ R. Bernhard,¹⁹ I. Bertram,³⁹ M. Besançon,¹⁵ R. Beuselinck,⁴⁰ P. C. Bhat,⁴⁵ S. Bhatia,⁵⁸ V. Bhatnagar,²³ G. Blazey,⁴⁷ S. Blessing,⁴⁴ K. Bloom,⁵⁹ A. Boehnlein,⁴⁵ D. Boline,⁶⁴ E. E. Boos,³³ G. Borissov,³⁹ M. Borysova,³⁸¹ A. Brandt,⁷⁰ O. Brandt,²⁰ R. Brock,⁵⁷ A. Bross,⁴⁵ D. Brown,¹⁴ X. B. Bu,⁴⁵ M. Buehler,⁴⁵ V. Buescher,²¹ V. Bunichev,³³ S. Burdin,^{39b} C. P. Buszello,³⁷ E. Camacho-Pérez,²⁸ B. C. K. Casey,⁴⁵ H. Castilla-Valdez,²⁸ S. Caughron,⁵⁷ S. Chakrabarti,⁶⁴ K. M. Chan,⁵¹ A. Chandra,⁷² E. Chapon,¹⁵ G. Chen,⁵³ S. W. Cho,²⁷ S. Choi,²⁷ B. Choudhary,²⁴ S. Cihangir,⁴⁵ D. Claes,⁵⁹ J. Clutter,⁵³ M. Cooke,^{45k} W. E. Cooper,⁴⁵ M. Corcoran,⁷² F. Couderc,¹⁵ M.-C. Cousinou,¹² J. Cuth,²¹ D. Cutts,⁶⁹ A. Das,⁷¹ G. Davies,⁴⁰ S. J. de Jong,^{29,30} E. De La Cruz-Burelo,²⁸ F. Déliot,¹⁵ R. Demina,⁶³ D. Denisov,⁴⁵ S. P. Denisov,³⁴ S. Desai,⁴⁵ C. Deterre,^{41c} K. DeVaughan,⁵⁹ H. T. Diehl,⁴⁵ M. Diesburg,⁴⁵ P. F. Ding,⁴¹ A. Dominguez,⁵⁹ A. Dubey,²⁴ L. V. Dudko,³³ A. Duperrin,¹² S. Dutt,²³ M. Eads,⁴⁷ D. Edmunds,⁵⁷ J. Ellison,⁴³ V. D. Elvira,⁴⁵ Y. Enari,¹⁴ H. Evans,⁴⁹ A. Evdokimov,⁴⁶ V. N. Evdokimov,³⁴ A. Fauré,¹⁵ L. Feng,⁴⁷ T. Ferbel,⁶³ F. Fiedler,²¹ F. Filthaut,^{29,30} W. Fisher,⁵⁷ H. E. Fisk,⁴⁵ M. Fortner,⁴⁷ H. Fox,³⁹ S. Fuess,⁴⁵ P. H. Garbincius,⁴⁵ A. García-Bellido,⁶³ J. A. García-González,²⁸ V. Gavrilov,³² W. Geng,^{12,57} C. E. Gerber,⁴⁶ Y. Gershtein,⁶⁰ G. Ginther,^{45,63} O. Gogota,³⁸ G. Golovanov,³¹ P. D. Grannis,⁶⁴ S. Greder,¹⁶ H. Greenlee,⁴⁵ G. Grenier,¹⁷ Ph. Gris,¹⁰ J.-F. Grivaz,¹³ A. Grohsjean,^{15c} S. Grünendahl,⁴⁵ M. W. Grünewald,²⁶ T. Guillemin,¹³ G. Gutierrez,⁴⁵ P. Gutierrez,⁶⁷ J. Haley,⁶⁸ L. Han,⁴ K. Harder,⁴¹ A. Harel,⁶³ J. M. Hauptman,⁵² J. Hays,⁴⁰ T. Head,⁴¹ T. Hebbeker,¹⁸ D. Hedin,⁴⁷ H. Hegab,⁶⁸ A. P. Heinson,⁴³ U. Heintz,⁶⁹ C. Hensel,¹ I. Heredia-De La Cruz,^{28d} K. Herner,⁴⁵ G. Hesketh,^{41f} M. D. Hildreth,⁵¹ R. Hirosky,⁷³ T. Hoang,⁴⁴ J. D. Hobbs,⁶⁴ B. Hoeneisen,⁹ J. Hogan,⁷² M. Hohlfeld,²¹ J. L. Holzbauer,⁵⁸ I. Howley,⁷⁰ Z. Hubacek,^{7,15} V. Hynek,⁷ I. Iashvili,⁶² Y. Ilchenko,⁴¹ R. Illingworth,⁴⁵ A. S. Ito,⁴⁵ S. Jabeen,^{45m} M. Jaffré,¹³ A. Jayasinghe,⁶⁷ M. S. Jeong,²⁷ R. Jesik,⁴⁰ P. Jiang,⁴ K. Johns,⁴² E. Johnson,⁵⁷ M. Johnson,⁴⁵ A. Jonckheere,⁴⁵ P. Jonsson,⁴⁰ J. Joshi,⁴³ A. W. Jung,⁴⁵ A. Juste,³⁶ E. Kajfasz,¹² D. Karmanov,³³ I. Katsanos,⁵⁹ M. Kaur,²³ R. Kehoe,⁷¹ S. Kermiche,¹² N. Khalatyan,⁴⁵ A. Khanov,⁶⁸ A. Kharchilava,⁶² Y. N. Kharzheev,³¹ I. Kiselevich,³² J. M. Kohli,²³ A. V. Kozelov,³⁴ J. Kraus,⁵⁸ A. Kumar,⁶² A. Kupco,⁸ T. Kurča,¹⁷ V. A. Kuzmin,³³ S. Lammers,⁴⁹ P. Lebrun,¹⁷ H. S. Lee,²⁷ S. W. Lee,⁵² W. M. Lee,⁴⁵ X. Lei,⁴² J. Lellouch,¹⁴ D. Li,¹⁴ H. Li,⁷³ L. Li,⁴³ Q. Z. Li,⁴⁵ J. K. Lim,²⁷ D. Lincoln,⁴⁵ J. Linnemann,⁵⁷ V. V. Lipaev,³⁴ R. Lipton,⁴⁵ H. Liu,⁷¹ Y. Liu,⁴ A. Lobodenko,³⁵ M. Lokajicek,⁸ R. Lopes de Sa,⁴⁵ R. Luna-Garcia,^{28g} A. L. Lyon,⁴⁵ A. K. A. Maciel,¹ R. Madar,¹⁹ R. Magaña-Villalba,²⁸ S. Malik,⁵⁹ V. L. Malyshev,⁴⁷ J. Mansour,²⁰ J. Martínez-Ortega,²⁸ R. McCarthy,⁶⁴ C. L. McGivern,⁴¹ M. M. Meijer,^{29,30} A. Melnitchouk,⁴⁵ D. Menezes,⁴⁷ P. G. Mercadante,³ M. Merkin,³³ A. Meyer,¹⁸ J. Meyer,²⁰ⁱ F. Miconi,¹⁶ N. K. Mondal,²⁵ M. Mulhearn,⁷³ E. Nagy,¹² M. Narain,⁶⁹ R. Nayyar,⁴² H. A. Neal,⁵⁶ J. P. Negret,⁵ P. Neustroev,³⁵ H. T. Nguyen,⁷³ T. Nunnemann,²² J. Orduna,⁷² N. Osman,¹² J. Osta,⁵¹ A. Pal,⁷⁰ N. Parashar,⁵⁰ V. Parihar,⁶⁹ S. K. Park,²⁷ R. Partridge,^{69e} N. Parua,⁴⁹ A. Patwa,^{65j} B. Penning,⁴⁰ M. Perfilov,³³ Y. Peters,⁴¹ K. Petridis,⁴¹ G. Petrillo,⁶³ P. Pétrouff,¹³ M.-A. Pleier,⁶⁵ V. M. Podstavkov,⁴⁵ A. V. Popov,³⁴ M. Prewitt,⁷² D. Price,⁴¹ N. Prokopenko,³⁴ J. Qian,⁵⁶ A. Quadt,²⁰ B. Quinn,⁵⁸ P. N. Ratoff,³⁹ I. Razumov,³⁴ I. Ripp-Baudot,¹⁶ F. Rizatdinova,⁶⁸ M. Rominsky,⁴⁵ A. Ross,³⁹ C. Royon,¹⁵ P. Rubinov,⁴⁵ R. Ruchti,⁵¹ G. Sajot,¹¹ A. Sánchez-Hernández,²⁸ M. P. Sanders,²² A. S. Santos,^{1h} G. Savage,⁴⁵ M. Savitskiy,³⁸ L. Sawyer,⁵⁴ T. Scanlon,⁴⁰ R. D. Schamberger,⁶⁴ Y. Scheglov,³⁵ H. Schellman,⁴⁸ M. Schott,²¹ C. Schwanenberger,⁴¹ R. Schwienhorst,⁵⁷ J. Sekaric,⁵³ H. Severini,⁶⁷ E. Shabalina,²⁰ V. Shary,¹⁵ S. Shaw,⁴¹ A. A. Shchukin,³⁴ V. Simak,⁷ P. Skubic,⁶⁷ P. Slattery,⁶³ D. Smirnov,⁵¹ G. R. Snow,⁵⁹ J. Snow,⁶⁶ S. Snyder,⁶⁵ S. Söldner-Rembold,⁴¹ L. Sonnenschein,¹⁸ K. Soustruznik,⁶ J. Stark,¹¹ D. A. Stoyanova,³⁴ M. Strauss,⁶⁷ L. Suter,⁴¹ P. Svoisky,⁶⁷ M. Titov,¹⁵ V. V. Tokmenin,³¹ Y.-T. Tsai,⁶³ D. Tsybychev,⁶⁴ B. Tuchming,¹⁵ C. Tully,⁶¹ L. Uvarov,³⁵ S. Uvarov,³⁵ S. Uzunyan,⁴⁷ R. Van Kooten,⁴⁹ W. M. van Leeuwen,²⁹ N. Varelas,⁴⁶ E. W. Varnes,⁴² I. A. Vasilyev,³⁴ A. Y. Verkheev,³¹ L. S. Vertogradov,³¹ M. Verzocchi,⁴⁵ M. Vesterinen,⁴¹ D. Vilanova,¹⁵ P. Vokac,⁷ H. D. Wahl,⁴⁴ M. H. L. S. Wang,⁴⁵ J. Warchol,⁵¹ G. Watts,⁷⁴ M. Wayne,⁵¹ J. Weichert,²¹ L. Welty-Rieger,⁴⁸ M. R. J. Williams,⁴⁹ⁿ G. W. Wilson,⁵³ M. Wobisch,⁵⁴ D. R. Wood,⁵⁵ T. R. Wyatt,⁴¹ Y. Xie,⁴⁵ R. Yamada,⁴⁵ S. Yang,⁴ T. Yasuda,⁴⁵ Y. A. Yatsunenko,³¹ W. Ye,⁶⁴ Z. Ye,⁴⁵ H. Yin,⁴⁵ K. Yip,⁶⁵ S. W. Youn,⁴⁵ J. M. Yu,⁵⁶ J. Zennamo,⁶² T. G. Zhao,⁴¹ B. Zhou,⁵⁶ J. Zhu,⁵⁶ M. Zielinski,⁶³ D. Zieminska,⁴⁹ and L. Zivkovic¹⁴

(D0 Collaboration)

¹LAFEX, Centro Brasileiro de Pesquisas Físicas, Rio de Janeiro, Brazil²Universidade do Estado do Rio de Janeiro, Rio de Janeiro, Brazil³Universidade Federal do ABC, Santo André, Brazil⁴University of Science and Technology of China, Hefei, People's Republic of China⁵Universidad de los Andes, Bogotá, Colombia

- ⁶Charles University, Faculty of Mathematics and Physics, Center for Particle Physics, Prague, Czech Republic
- ⁷Czech Technical University in Prague, Prague, Czech Republic
- ⁸Institute of Physics, Academy of Sciences of the Czech Republic, Prague, Czech Republic
- ⁹Universidad San Francisco de Quito, Quito, Ecuador
- ¹⁰LPC, Université Blaise Pascal, CNRS/IN2P3, Clermont, France
- ¹¹LPSC, Université Joseph Fourier Grenoble 1, CNRS/IN2P3, Institut National Polytechnique de Grenoble, Grenoble, France
- ¹²CPPM, Aix-Marseille Université, CNRS/IN2P3, Marseille, France
- ¹³LAL, Université Paris-Sud, CNRS/IN2P3, Orsay, France
- ¹⁴LPNHE, Universités Paris VI and VII, CNRS/IN2P3, Paris, France
- ¹⁵CEA, Irfu, SPP, Saclay, France
- ¹⁶IPHC, Université de Strasbourg, CNRS/IN2P3, Strasbourg, France
- ¹⁷IPNL, Université Lyon 1, CNRS/IN2P3, Villeurbanne, France and Université de Lyon, Lyon, France
- ¹⁸III. Physikalisches Institut A, RWTH Aachen University, Aachen, Germany
- ¹⁹Physikalisches Institut, Universität Freiburg, Freiburg, Germany
- ²⁰II. Physikalisches Institut, Georg-August-Universität Göttingen, Göttingen, Germany
- ²¹Institut für Physik, Universität Mainz, Mainz, Germany
- ²²Ludwig-Maximilians-Universität München, München, Germany
- ²³Panjab University, Chandigarh, India
- ²⁴Delhi University, Delhi, India
- ²⁵Tata Institute of Fundamental Research, Mumbai, India
- ²⁶University College Dublin, Dublin, Ireland
- ²⁷Korea Detector Laboratory, Korea University, Seoul, Korea
- ²⁸CINVESTAV, Mexico City, Mexico
- ²⁹Nikhef, Science Park, Amsterdam, the Netherlands
- ³⁰Radboud University Nijmegen, Nijmegen, the Netherlands
- ³¹Joint Institute for Nuclear Research, Dubna, Russia
- ³²Institute for Theoretical and Experimental Physics, Moscow, Russia
- ³³Moscow State University, Moscow, Russia
- ³⁴Institute for High Energy Physics, Protvino, Russia
- ³⁵Petersburg Nuclear Physics Institute, St. Petersburg, Russia
- ³⁶Institució Catalana de Recerca i Estudis Avançats (ICREA) and Institut de Física d'Altes Energies (IFAE), Barcelona, Spain
- ³⁷Uppsala University, Uppsala, Sweden
- ³⁸Taras Shevchenko National University of Kyiv, Kiev, Ukraine
- ³⁹Lancaster University, Lancaster LA1 4YB, United Kingdom
- ⁴⁰Imperial College London, London SW7 2AZ, United Kingdom
- ⁴¹The University of Manchester, Manchester M13 9PL, United Kingdom
- ⁴²University of Arizona, Tucson, Arizona 85721, USA
- ⁴³University of California Riverside, Riverside, California 92521, USA
- ⁴⁴Florida State University, Tallahassee, Florida 32306, USA
- ⁴⁵Fermi National Accelerator Laboratory, Batavia, Illinois 60510, USA
- ⁴⁶University of Illinois at Chicago, Chicago, Illinois 60607, USA
- ⁴⁷Northern Illinois University, DeKalb, Illinois 60115, USA
- ⁴⁸Northwestern University, Evanston, Illinois 60208, USA
- ⁴⁹Indiana University, Bloomington, Indiana 47405, USA
- ⁵⁰Purdue University Calumet, Hammond, Indiana 46323, USA
- ⁵¹University of Notre Dame, Notre Dame, Indiana 46556, USA
- ⁵²Iowa State University, Ames, Iowa 50011, USA
- ⁵³University of Kansas, Lawrence, Kansas 66045, USA
- ⁵⁴Louisiana Tech University, Ruston, Louisiana 71272, USA
- ⁵⁵Northeastern University, Boston, Massachusetts 02115, USA
- ⁵⁶University of Michigan, Ann Arbor, Michigan 48109, USA
- ⁵⁷Michigan State University, East Lansing, Michigan 48824, USA
- ⁵⁸University of Mississippi, University, Mississippi 38677, USA
- ⁵⁹University of Nebraska, Lincoln, Nebraska 68588, USA
- ⁶⁰Rutgers University, Piscataway, New Jersey 08855, USA
- ⁶¹Princeton University, Princeton, New Jersey 08544, USA
- ⁶²State University of New York, Buffalo, New York 14260, USA

⁶³University of Rochester, Rochester, New York 14627, USA⁶⁴State University of New York, Stony Brook, New York 11794, USA⁶⁵Brookhaven National Laboratory, Upton, New York 11973, USA⁶⁶Langston University, Langston, Oklahoma 73050, USA⁶⁷University of Oklahoma, Norman, Oklahoma 73019, USA⁶⁸Oklahoma State University, Stillwater, Oklahoma 74078, USA⁶⁹Brown University, Providence, Rhode Island 02912, USA⁷⁰University of Texas, Arlington, Texas 76019, USA⁷¹Southern Methodist University, Dallas, Texas 75275, USA⁷²Rice University, Houston, Texas 77005, USA⁷³University of Virginia, Charlottesville, Virginia 22904, USA⁷⁴University of Washington, Seattle, Washington 98195, USA

(Received 22 July 2015; published 22 September 2015)

We present a simultaneous measurement of the forward-backward asymmetry and the top-quark polarization in $t\bar{t}$ production in dilepton final states using 9.7 fb^{-1} of proton-antiproton collisions at $\sqrt{s} = 1.96 \text{ TeV}$ with the D0 detector. To reconstruct the distributions of kinematic observables we employ a matrix element technique that calculates the likelihood of the possible $t\bar{t}$ kinematic configurations. After accounting for the presence of background events and for calibration effects, we obtain a forward-backward asymmetry of $A^{\bar{t}} = (15.0 \pm 6.4(\text{stat}) \pm 4.9(\text{syst}))\%$ and a top-quark polarization times spin analyzing power in the beam basis of $\kappa P = (7.2 \pm 10.5(\text{stat}) \pm 4.2(\text{syst}))\%$, with a correlation of -56% between the measurements. If we constrain the forward-backward asymmetry to its expected standard model value, we obtain a measurement of the top polarization of $\kappa P = (11.3 \pm 9.1(\text{stat}) \pm 1.9(\text{syst}))\%$. If we constrain the top polarization to its expected standard model value, we measure a forward-backward asymmetry of $A^{\bar{t}} = (17.5 \pm 5.6(\text{stat}) \pm 3.1(\text{syst}))\%$. A combination with the D0 $A^{\bar{t}}$ measurement in the lepton + jets final state yields an asymmetry of $A^{\bar{t}} = (11.8 \pm 2.5(\text{stat}) \pm 1.3(\text{syst}))\%$. Within their respective uncertainties, all these results are consistent with the standard model expectations.

DOI: [10.1103/PhysRevD.92.052007](https://doi.org/10.1103/PhysRevD.92.052007)

PACS numbers: 14.65.Ha, 12.38.Qk, 13.85.Qk, 11.30.Er

I. INTRODUCTION

In proton-antiproton collisions at $\sqrt{s} = 1.96 \text{ TeV}$, top-quark pairs are predominantly produced in valence quark-antiquark annihilations. The standard model (SM) predicts

this process to be slightly forward-backward asymmetric: the top quark (antiquark) tends to be emitted in the same direction as the incoming quark (antiquark), and thus, in the same direction as the incoming proton (antiproton). The forward-backward asymmetry in the production is mainly due to positive contributions from the interference between tree-level and next-to-leading-order (NLO) box diagrams. It receives smaller negative contributions from the interference between initial and final state radiation. The interferences with electroweak processes increase the asymmetry. In the SM, the asymmetry is predicted to be $\approx 10\%$ [1–3]. Within the SM, the longitudinal polarizations of the top quark and antiquark are due to parity violating electroweak contributions to the production process. The polarization is expected to be $< 0.5\%$ for all choices of the spin quantization axis [4,5].

^aVisitor from Augustana College, Sioux Falls, SD, USA.^bVisitor from the University of Liverpool, Liverpool, UK.^cVisitor from DESY, Hamburg, Germany.^dVisitor from CONACyT, Mexico City, Mexico.^eVisitor from SLAC, Menlo Park, CA, USA.^fVisitor from University College London, London, UK.^gVisitor from Centro de Investigacion en Computacion—IPN, Mexico City, Mexico.^hVisitor from Universidade Estadual Paulista, São Paulo, Brazil.ⁱVisitor from Karlsruher Institut für Technologie (KIT)—Steinbuch Centre for Computing (SCC), D-76128 Karlsruhe, Germany.^jVisitor from Office of Science, U.S. Department of Energy, Washington, D.C. 20585, USA.^kVisitor from American Association for the Advancement of Science, Washington, D.C. 20005, USA.^lVisitor from Kiev Institute for Nuclear Research, Kiev, Ukraine.^mVisitor from University of Maryland, College Park, Maryland 20742, USA.ⁿVisitor from European Organization for Nuclear Research (CERN), Geneva, Switzerland.

Physics beyond the SM could affect the $t\bar{t}$ production mechanism and thus both the forward-backward asymmetry and the top-quark and antiquark polarizations. In particular, models with a new parity violating interaction such as models with axiguons [6–9], can induce a large positive or negative asymmetry together with a sizable polarization.

The $t\bar{t}$ production asymmetry, $A^{\bar{t}}$, is defined in terms of the difference between the rapidities of the top and antitop quarks, $\Delta y_{t\bar{t}} = y_t - y_{\bar{t}}$:

$$A^{\bar{t}\bar{t}} = \frac{N(\Delta y_{\bar{t}\bar{t}} > 0) - N(\Delta y_{\bar{t}\bar{t}} < 0)}{N(\Delta y_{\bar{t}\bar{t}} > 0) + N(\Delta y_{\bar{t}\bar{t}} < 0)}, \quad (1)$$

where $N(X)$ is the number of events in configuration X . By definition, $A^{\bar{t}\bar{t}}$ is independent of effects from the top-quark decay such as top-quark polarization. However, it requires the reconstruction of the $\bar{t}\bar{t}$ initial state from the decay products, which is challenging especially in dilepton channels.

Measurements of $A^{\bar{t}\bar{t}}$ have been performed in the lepton + jets channels by the CDF [10] and D0 [11] Collaborations. Other asymmetry measurements have been performed using observables based on the pseudorapidity of the leptons from $t \rightarrow Wb \rightarrow \ell\nu b$ decays [12–15]. All these measurements agree with the SM predictions. A comprehensive review of asymmetry measurements performed at the Tevatron can be found in Ref. [16].

As top quarks decay before they hadronize, their spin properties are transferred to the decay products. The top (antitop) polarization $P_{\hat{n}}^+$ ($P_{\hat{n}}^-$) along a given quantization axis \hat{n} impacts the angular distribution of the positively (negatively) charged lepton [5]

$$\frac{d\sigma}{d\cos\theta^\pm} = \frac{1}{2}(1 + \kappa^\pm P_{\hat{n}}^\pm \cos\theta^\pm), \quad (2)$$

where θ^+ (θ^-) is the angle between the positively (negatively) charged lepton in the top (antitop) rest frame and the quantization axis \hat{n} , and κ^+ (κ^-) is the spin analyzing power of the positively (negatively) charged lepton, which is close to 1 (−1) at the 0.1% level within the SM [5]. The polarization terms $\kappa^+ P_{\hat{n}}^+$ ($\kappa^- P_{\hat{n}}^-$) can be obtained as two times the asymmetry of the $\cos\theta^+$ ($\cos\theta^-$) distribution

$$A_{\hat{n}}^{\ell^\pm} = \frac{N(\cos\theta^\pm > 0) - N(\cos\theta^\pm < 0)}{N(\cos\theta^\pm > 0) + N(\cos\theta^\pm < 0)}. \quad (3)$$

In the following we use the beam basis, where \hat{n} is the direction of the proton beam in the $\bar{t}\bar{t}$ zero momentum frame. Since we only use the beam basis, we omit the subscript \hat{n} in the following and define the polarization observable as

$$\kappa P = \frac{1}{2}(\kappa^+ P^+ - \kappa^- P^-) = A^{\ell^+} - A^{\ell^-}. \quad (4)$$

Polarization effects have been studied at the Tevatron in the context of the measurements of the leptonic asymmetries in Ref. [17], but no actual measurement of the polarization has been performed. Measurements of the polarization have been conducted for top pair production in pp collisions at the Large Hadron Collider at $\sqrt{s} = 7$ TeV. These measurements, performed in different basis choices, are all consistent with the SM expectations [18,19].

This article presents a simultaneous measurement of $A^{\bar{t}\bar{t}}$ and κP with the D0 detector in the dilepton decay channel. It is based on the full Tevatron integrated luminosity of 9.7 fb^{-1} using $\bar{t}\bar{t}$ final states with two leptons, ee , $e\mu$, or $\mu\mu$. We first reconstruct the $\Delta y_{\bar{t}\bar{t}}$ and $\cos\theta^\pm$ distributions employing a matrix element integration technique similar to that used for the top-quark mass measurement in the dilepton channel [20]. These distributions are used to extract raw measurements of asymmetry and polarization, $A_{\text{raw}}^{\bar{t}\bar{t}}$ and κP_{raw} , in data. The experimental observables $A_{\text{raw}}^{\bar{t}\bar{t}}$ and κP_{raw} are correlated because of acceptance and resolution effects. Using a MC@NLO [21,22] simulation, we compute the relation between the raw measurements $A_{\text{raw}}^{\bar{t}\bar{t}}$ and κP_{raw} , and the true parton-level asymmetry and polarization to determine calibration corrections. We then extract the final measured values of $A^{\bar{t}\bar{t}}$ and κP . This is the first measurement of the $\bar{t}\bar{t}$ forward-backward asymmetry obtained from the reconstructed $\Delta y_{\bar{t}\bar{t}}$ distribution in the dilepton channel and the first measurement of the top-quark polarization at the Fermilab Tevatron collider.

II. DETECTOR AND OBJECT RECONSTRUCTION

The D0 detector used for the Run II of the Fermilab Tevatron collider is described in detail in Refs. [23–26]. The innermost part of the detector is composed of a central tracking system with a silicon microstrip tracker and a central fiber tracker embedded within a 2 T solenoidal magnet. The tracking system is surrounded by a central preshower detector and a liquid-argon/uranium calorimeter with electromagnetic, fine hadronic, and coarse hadronic sections. The central calorimeter (CC) covers pseudorapidities [27] of $|\eta| \lesssim 1.1$. Two end calorimeters (EC) extend the coverage to $|\eta| \lesssim 4.2$, while the coverage of the pseudorapidity region $1.1 \leq |\eta| \leq 1.5$, where the EC and CC overlap, is augmented with scintillating tiles. A muon spectrometer, with pseudorapidity coverage of $|\eta| \lesssim 2$, is located outside the calorimetry and comprises drift tubes and scintillation counters, before and after iron toroidal magnets. Trigger decisions are based on information from the tracking detectors, calorimeters, and muon spectrometer.

Electrons are reconstructed as isolated clusters in the electromagnetic calorimeter and required to spatially match a track in the central tracking system. They have to pass a boosted decision tree [28] criterion based on calorimeter shower shape observables, calorimeter isolation, a spatial track match probability estimate, and the ratio of the electron cluster energy to track momentum (E/p). Electrons are required to be in the acceptance of the electromagnetic calorimeter ($|\eta| < 1.1$ or $1.5 < |\eta| < 2.5$).

Muons are identified by the presence of at least one track segment reconstructed in the acceptance ($|\eta| < 2.0$) of the muon spectrometer that is spatially consistent with a track in the central tracking detector [29]. The transverse

momentum and charge are measured by the curvature in the central tracking system. The angular distance to the nearest jet, the momenta of charged particles in a cone around the muon track, and the energy deposited around the muon trajectory in the calorimeter, are used to select isolated muons.

Jets are reconstructed from energy deposits in the calorimeter using an iterative midpoint cone algorithm [30] with a cone radius of $\mathcal{R} = 0.5$ [31]. The jet energies are calibrated using transverse momentum balance in $\gamma + \text{jet}$ events [32].

III. DATA SET AND EVENT SELECTION

The signature of $t\bar{t}$ production in dilepton final states consists of two high- p_T leptons (electrons or muons), two high- p_T jets arising from the showering of two b quarks, and missing transverse energy (\cancel{E}_T) due to the undetected neutrinos. The main backgrounds in this final state arise from $Z \rightarrow \ell\ell$, with $\ell = e, \mu$, or τ , and diboson production (WW, WZ, ZZ). These backgrounds are evaluated from Monte Carlo (MC) simulated samples as described in Sec. IV C. Another source of background comes from $W + \text{jets}$ and multijet events, if one or two jets are misreconstructed as electrons or if a muon from a jet passes the isolation criteria. The contribution from these backgrounds, denoted as ‘‘instrumental background events,’’ are estimated directly from data as described in Sec. IV E. Each of the dilepton channels is subject to a different mixture and level of background contamination, in particular for the background arising from the $Z \rightarrow \ell\ell$ process. We therefore apply slightly different selection requirements. The main selection criteria to obtain the final samples of $t\bar{t}$ candidate events are

- (1) We select two high- p_T ($p_T > 15$ GeV) isolated leptons of opposite charge.
- (2) We require that at least one electron passes a single electron trigger condition in the ee channel ($\approx 100\%$ efficient), and that at least one muon passes a single muon trigger condition in the $\mu\mu$ channel ($\approx 85\%$ efficient). In the $e\mu$ channel, we do not require any specific trigger condition, i.e., we use all D0 trigger terms ($\approx 100\%$ efficient).
- (3) We require two or more jets of $p_T > 20$ GeV and $|\eta| < 2.5$.

- (4) We further improve the purity of the selection by exploiting the significant imbalance of transverse energy due to undetected neutrinos and by exploiting several topological variables:
 - (i) The missing transverse energy \cancel{E}_T is the magnitude of the missing transverse momentum, obtained from the vector sum of the transverse components of energy deposits in the calorimeter, corrected for the differences in detector response of the reconstructed muons, electrons, and jets.
 - (ii) The missing transverse energy significance, E_T^{sig} , is the logarithm of the probability to measure \cancel{E}_T under the hypothesis that the true missing transverse momentum is zero, accounting for the energy resolution of individual reconstructed objects and underlying event [33].
 - (iii) H_T is the scalar sum of transverse momenta of the leading lepton and the two leading jets.

In the ee channel we require $E_T^{\text{sig}} \geq 5$, in the $e\mu$ channel $H_T > 110$ GeV, and in the $\mu\mu$ channel $E_T^{\text{sig}} \geq 5$ and $\cancel{E}_T > 40$ GeV.

- (5) We require that at least one of the two leading jets be b tagged, using a cut on the multivariate discriminant described in Ref. [34]. The requirement is optimized separately for each channel. The $t\bar{t}$ selection efficiencies for these requirements are $\approx 82\%$, $\approx 83\%$, and $\approx 75\%$ for the $ee, e\mu,$ and $\mu\mu$ channels, respectively.
- (6) The integration of the matrix elements by VEGAS, described in Sec. V A, may return a tiny probability if the event is not consistent with the $t\bar{t}$ event hypothesis due to numerical instabilities in the integration process. After removing low probability events, we retain signal events in the MC simulation with an efficiency of 99.97%. For background MC, the efficiency is $> 99.3\%$. We remove no data events with this requirement.

IV. SIGNAL AND BACKGROUND SAMPLES

A. Signal

To simulate the $t\bar{t}$ signal, we employ MC events generated with the CTEQ6M1 parton distribution functions

TABLE I. Comparison between expected and observed numbers of events at the final selection level for the different channels. The values are reported with their statistical uncertainties.

Channel	$Z \rightarrow \ell\ell$	Dibosons	Instrumental	$t\bar{t} \rightarrow \ell\ell jj$	Total Expected	Data	$\frac{\text{Data}}{\text{Expected}}$
$\mu\mu$	$10.65^{+0.5}_{-0.5}$	$1.7^{+0.1}_{-0.1}$	$0.0^{+0.0}_{-0.0}$	$79.3^{+0.6}_{-0.6}$	$91.7^{+0.7}_{-0.7}$	92	1.00 ± 0.10
$e\mu$	$13.03^{+0.5}_{-0.5}$	$3.7^{+0.2}_{-0.2}$	$16.4^{+0.7}_{-0.7}$	$283.1^{+1.0}_{-1.0}$	$316.2^{+1.3}_{-1.3}$	346	1.09 ± 0.05
ee	$12.92^{+0.4}_{-0.4}$	$1.9^{+0.1}_{-0.1}$	$1.8^{+0.08}_{-0.08}$	$95.5^{+0.6}_{-0.6}$	$112.1^{+0.8}_{-0.8}$	104	0.92 ± 0.10

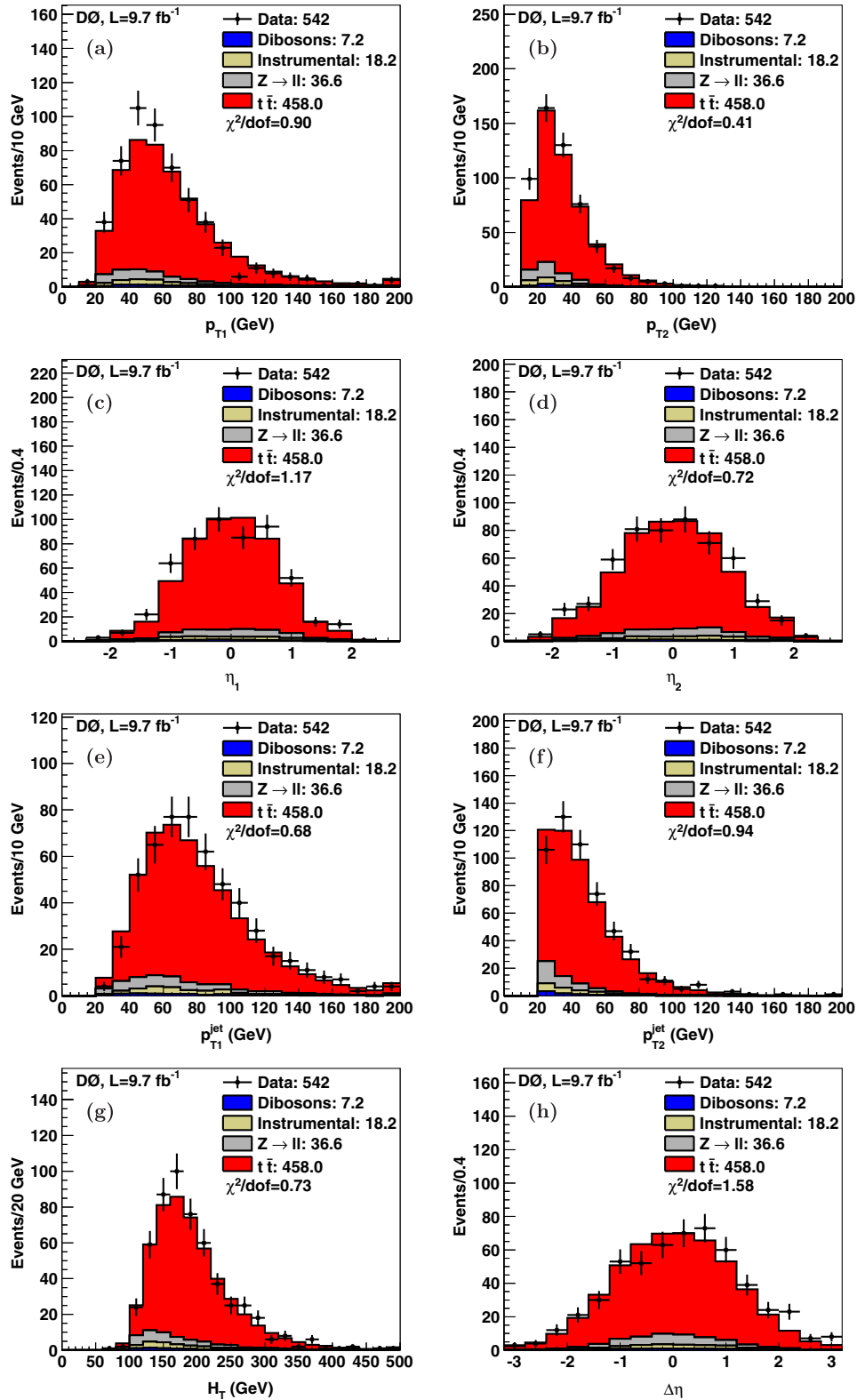


FIG. 1 (color online). Comparison of distributions between data and MC simulations at the final selection for (a) the transverse momentum of the leading lepton, (b) the transverse momentum of the secondary lepton, (c) the pseudorapidity of the leading lepton, (d) the pseudorapidity of the secondary lepton, (e) the transverse momentum of the leading jet, (f) the transverse momentum of the secondary jet, (g) the H_T , and (h) the difference between the two lepton pseudorapidities. The overflow bin content has been added to the last bin.

(PDFs) [35] and MC@NLO 3.4 [21,22] interfaced to HERWIG 6.510 [36] for showering and hadronization. Alternate signal MC samples are generated to study systematic uncertainties and the shape of the $\Delta y_{\bar{t}t}$ distribution. We use a sample generated with ALPGEN [37] interfaced to PYTHIA 6.4 [38] for showering and hadronization and a sample generated with ALPGEN interfaced to HERWIG 6.510. For both samples we use CTEQ6L1 PDFs [35].

The MC@NLO generator is used for the nominal signal sample as it simulates NLO effects yielding nonzero $A^{\bar{t}t}$. The value of $A^{\bar{t}t}$ at parton level without applying any selection requirement is $A^{\bar{t}t} = (5.23 \pm 0.07(\text{stat}))\%$, which is smaller than a SM prediction [2] that includes higher order effects.

The MC events are generated with a top-quark mass of $m_t = 172.5$ GeV. They are normalized to a $\bar{t}t$ production cross section of 7.45 pb, which corresponds to the calculation of Ref. [39] for $m_t = 172.5$ GeV. The generated top mass of 172.5 GeV differs from the Tevatron average mass of 173.18 ± 0.94 GeV [40]. We correct for this small difference in Sec. VI B.

B. Beyond standard model benchmarks

We also study the five benchmark axigluons models proposed in Ref. [41] that modify $\bar{t}t$ production. For each of the proposed beyond standard model (BSM) benchmarks, we produce a $\bar{t}t$ MC sample using the MadGraph [42] generator interfaced to PYTHIA 6.4 for showering and hadronization, and the CTEQ6L1 PDFs. The Z' boson model proposed in Ref. [41] is not considered here since it is excluded by our $\bar{t}t$ differential cross-section measurement [43].

C. Background estimated with simulated events

The background samples are generated using the CTEQ6L1 PDFs. The $Z \rightarrow \ell\ell$ events are generated using ALPGEN interfaced to PYTHIA 6.4. We normalize the $Z \rightarrow \ell\ell$ sample to the next-to-next-to-leading-order cross section [44]. The p_T distribution of Z bosons is weighted to match the distribution observed in data [45], taking into account its dependence on the number of reconstructed jets. The diboson backgrounds are simulated using PYTHIA and are normalized to the NLO cross-section calculation performed by MCFM [46,47].

D. D0 simulation

The signal and background processes except instrumental background are simulated with a detailed GEANT3-based [48] MC simulation of the D0 detector. They are processed with the same reconstruction software as used for data. In order to model the effects of multiple $p\bar{p}$ interactions, the MC events are overlaid with events from random $p\bar{p}$ collisions with the same luminosity distribution as data. The jet energy calibration is adjusted in simulated events to

match the one measured in data. Corrections for residual differences between data and simulation are applied to electrons, muons, and jets for both identification efficiencies and energy resolutions.

E. Instrumental background estimated with data

The normalization of events with jets misidentified as electrons is estimated using the “matrix method” [49] separately for the ee and $e\mu$ channels. The contribution from jets producing identified muons in the $\mu\mu$ channel is obtained using the same selection criteria as for the sample of $\bar{t}t$ candidate events, but demanding that the leptons have the same charge. In the $e\mu$ channel, it is obtained in the same way but after subtracting the contribution from events with jets misidentified as electrons.

Once the absolute contribution of instrumental background events has been determined, we also need “template samples” that model their kinematic properties. In the $e\mu$ channel, the template for instrumental background events is obtained with the same selection criteria as for the samples of $\bar{t}t$ candidate events, but without applying the complete set of electron selection criteria. For the $\mu\mu$ and ee channels, the contributions from instrumental background events is negligible and the result is not sensitive to the choice of template. For simplicity, we reemploy the $e\mu$ template for both the $\mu\mu$ and ee channels.

F. Comparison of MC simulation to selected data

A comparison between the expected and observed numbers of events at the final selection levels is reported in Table I. The selected sample is relatively pure with a background fraction varying between 10% and 16% depending on the channel. A comparison of kinematic distributions between data and expectations at the final selection level is shown in Fig. 1.

V. MATRIX ELEMENT METHOD

To reconstruct distributions of kinematic observables describing the $\bar{t}t$ events, we use a novel modification of the matrix element (ME) integration developed for the m_t measurements [20,50] by the D0 Collaboration. In particular, this method is employed to reconstruct the $\Delta y_{\bar{t}t}$, $\cos(\theta^+)$, and $\cos(\theta^-)$ distributions, from which an estimate of the forward-backward asymmetry and top polarization are extracted.

A. Matrix element integration

The ME integration used in Refs. [20,50] consists in computing the likelihood L_z to observe a given event with the vector of measured quantities z ,

$$L_z = \frac{1}{\mathcal{A} \cdot \sigma_{\text{tot}}} \sum_{\text{flavors}} \int_{x, q_1, q_2, p_T^{\bar{t}}, \phi^{\bar{t}}} f_{\text{PDF}}(q_1) f_{\text{PDF}}(q_2) W(p_T^{\bar{t}}) \times W(x, z) \frac{(2\pi)^4 |\mathcal{M}|^2}{4\sqrt{(q_1 \cdot q_2)^2}} d\Phi_6 dp_T^{\bar{t}} d\phi^{\bar{t}} dq_1 dq_2. \quad (5)$$

In this expression, x is a vector describing the kinematic quantities of the six particles of the $p\bar{p} \rightarrow t\bar{t} \rightarrow \ell^+\nu b\ell^-\bar{\nu}\bar{b}$ final state, \mathcal{M} is the matrix element describing the dynamics of the process, $d\Phi_6$ is the 6-body phase space term, the functions f_{PDF} are the PDFs of the incoming partons of momenta q_1 and q_2 and of different possible flavors, $W(x, z)$, referred to as the *transfer function*, describes the probability density of a parton state x to be reconstructed as z , $W(p_T^{\bar{t}})$ is a function describing the distribution of the $t\bar{t}$ system transverse momentum, $p_T^{\bar{t}}$, while the azimuthal angle of this system, $\phi^{\bar{t}}$, is assumed to have a uniform distribution over $[0, 2\pi]$, and $\mathcal{A} \cdot \sigma_{\text{tot}}$ is the product of the experimental acceptance and the production cross section. The matrix element, \mathcal{M} , is computed at leading order (LO) for $q\bar{q}$ annihilation only, as it represents the main subprocess ($\approx 85\%$) of the total $t\bar{t}$ production. The functions f_{PDF} are given by the CTEQ6M1 leading order PDF set. The function $W(p_T^{\bar{t}})$ is derived from parton-level simulated events generated with ALPGEN interfaced to PYTHIA. More details on this function can be found in Ref. [51]. Ambiguities between partons and reconstructed particle assignments are properly treated by defining an effective transfer function that sums over all the different assignments. As we consider only the two leading jets in the integration process, there are only two possibilities to assign a given jet to either the b or \bar{b} partons.

The number of variables to integrate is given by the six three-vectors of final state partons (of known mass), the $t\bar{t}$ transverse momentum and transverse direction, and the longitudinal momenta of the two incoming partons. These 22 integration variables are reduced by the following constraints: the lepton and b -quark directions are assumed to be perfectly measured (8 constraints), the energy-momentum between the initial state and the final state is conserved (4 constraints), the $\ell^+\nu$ and $\ell^-\bar{\nu}$ system have a mass of $M_W = 80.4$ GeV [52] (2 constraints), and the $\ell^+\nu b$ and $\ell^-\bar{\nu}\bar{b}$ system have a mass of $m_t = 172.5$ GeV (2 constraints). Transfer functions account for muon and jet energies. The transfer functions are the same as used in Ref. [50]. The electron momentum measurement has a precision of $\approx 3\%$, which is much better than the muon momentum resolution of typically 10% and the jet momentum resolution of typically 20%. We thus consider that the electron momenta are perfectly measured. This gives one additional constraint in the $e\mu$ channel and two additional constraints in the ee channel. Thus, we integrate over 4, 5, and 6 variables in the ee , $e\mu$, and $\mu\mu$ channels, respectively. The integration variables are $p_T^{\bar{t}}$, $\phi^{\bar{t}}$, energy of leading jet,

energy of subleading jet, and energy of the muon(s) (if applicable).

The integration is performed using the MC-based numerical integration program VEGAS [53,54]. The interface to the VEGAS integration algorithm is provided by the GNU Scientific Library [55]. The MC integration consists of randomly sampling the space of integration variables, computing a weight for each of the random points that accounts for both the integrand and the elementary volume of the sampling space, and finally summing all of the weights. The random sampling is based on a grid in the space of integration that is iteratively optimized to ensure fine sampling in regions with large variations of the integrand. For each of the random points, equations are solved to transform these integration variables into the parton-level variables of Eq. (5), accounting for the measured quantities z . The Jacobian of the transformation is also computed to ensure proper weighting of the sampling space elementary volume.

B. Likelihood of a parton-level observable

For any kinematic quantity K reconstructed from the parton momenta x , for example $K(x) = y_t - y_{\bar{t}}$, we can build a probability density $L_z(K)$ that measures the likelihood of $K(x)$ at the partonic level to give the reconstructed value K . This likelihood is obtained by inserting a term $\delta(K(x) - K)$ in the integrand of Eq. (5), and normalizing the function so that $\int L_z(K) dK = 1$. The probability density is obtained by modifying the VEGAS integration algorithm. For each reconstructed $t\bar{t}$ event and each point in the integration space tested by VEGAS, the integrand of Eq. (5) and the quantity K are computed. After the full space of integration has been sampled, we obtain a weighted distribution of the variable K that represents the function $L_z(K)$ up to an overall normalization factor.

For each reconstructed event with observed kinematics z_i , where i is an event index, we obtain a likelihood function $L_{z_i}(K)$. By accumulating these likelihood functions over the sample of events, we obtain a distribution that estimates the true distribution of the variable K . The performance of this method of reconstruction for parton-level distributions is estimated by comparing the accumulation of likelihood functions to the true parton-level quantities for MC events, as shown in Fig. 2.

C. Raw estimate of $A^{\bar{t}}$

We could choose to use the maximum of the likelihood function $L_z(\Delta y_{\bar{t}})$ to estimate the true value of $\Delta y_{\bar{t}}$ on an event-by-event basis. However, to maximize the use of available information, we keep the full shape of the L_z functions and accumulate these functions over the sample of $t\bar{t}$ events to obtain an estimate of the parton-level distributions, which is then used to determine $A^{\bar{t}}$. This method has been verified to perform better than

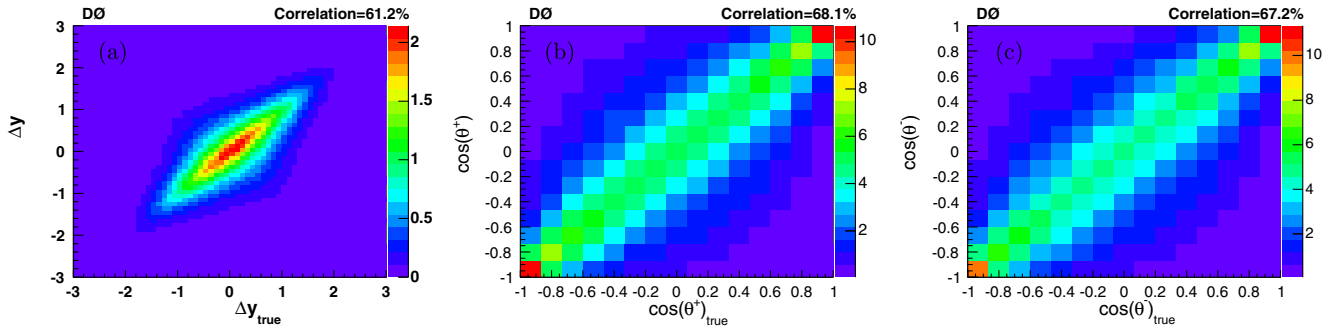


FIG. 2 (color online). Accumulation of likelihood functions [$\sum_{\text{events}} L_{z_i}(K)$, with K along the vertical axis] versus the corresponding true parton-level quantity (K_{true} along the horizontal axis) in $i\bar{i}$ MC events after applying the selection criteria for (a) $K = \Delta y_{i\bar{i}}$, (b) $K = \cos \theta^+$, and (c) $K = \cos \theta^-$. Each single MC event i contributes in these plots with a complete distribution, $L_{z_i}(X)$, along the vertical axis for a given value on the horizontal axis, K_{true} . The shades of color indicate the bin contents in arbitrary units.

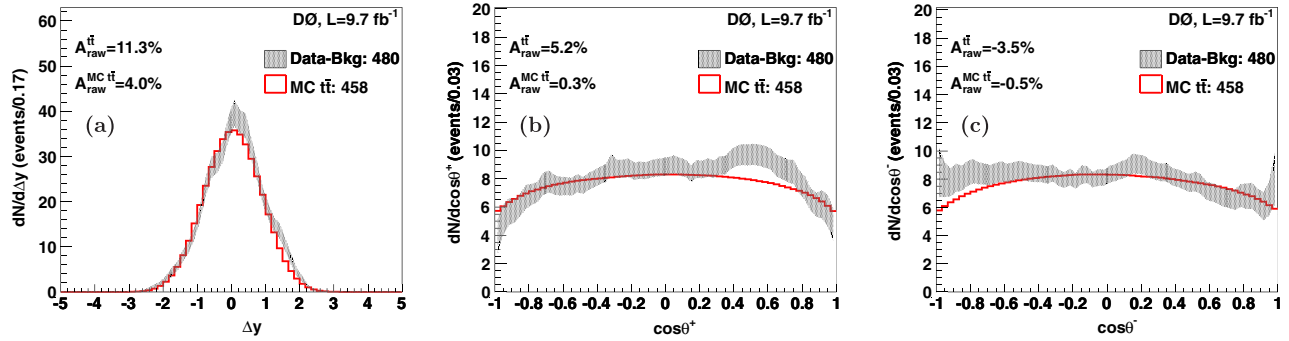


FIG. 3 (color online). Estimated distribution of the (a) $\Delta y_{i\bar{i}}$, (b) $\cos \theta^+$, and (c) $\cos \theta^-$ observables in dilepton events after subtracting the expected background contribution. Deviations between the background-subtracted data and MC can be attributed to statistical fluctuations. The background-subtracted data asymmetries and the MC asymmetries extracted from these distributions are also reported. These raw asymmetries need to be corrected for calibration effects to retrieve the parton-level asymmetries.

the maximum likelihood method. The distribution $\sum_{\text{events}} L_{z_i}(\Delta y_{i\bar{i}})$ is shown in Fig. 3(a), after subtracting the background contributions from the data. The raw asymmetry $A_{\text{raw}}^{i\bar{i}}$, extracted from this distribution, is reported in Table II. Since this $\Delta y_{i\bar{i}}$ distribution is an approximate estimation of the true distribution of $\Delta y_{i\bar{i}}$, the raw asymmetry $A_{\text{raw}}^{i\bar{i}}$ is an approximation of the true $A^{i\bar{i}}$. The measurement therefore needs to be calibrated. The calibration is discussed below.

TABLE II. Raw forward-backward asymmetry in data before background subtraction, $A_{\text{raw}}^{\text{data}}$, asymmetry of the background, $A_{\text{raw}}^{\text{bkg}}$, and measurement once the background contribution has been subtracted, $A_{\text{raw}}^{i\bar{i}}$. Asymmetries are reported in percent, together with their statistical uncertainties.

Channel	$A_{\text{raw}}^{\text{data}}$	$A_{\text{raw}}^{\text{bkg}}$	$A_{\text{raw}}^{i\bar{i}} = A_{\text{raw}}^{\text{data-bkg}}$
$e\mu$	9.2 ± 3.8	0.3 ± 1.9	10.1 ± 4.2
ee	15.8 ± 6.4	0.1 ± 2.0	18.8 ± 7.6
$\mu\mu$	6.7 ± 7.9	-0.3 ± 3.3	7.8 ± 9.1
Dilepton	10.1 ± 3.0	0.1 ± 1.1	11.3 ± 3.4

The use of an event-by-event likelihood function allows us to define an asymmetry observable for each event

$$A = \int_0^{\infty} L_z(\Delta y_{i\bar{i}}) d\Delta y_{i\bar{i}} - \int_{-\infty}^0 L_z(\Delta y_{i\bar{i}}) d\Delta y_{i\bar{i}}, \quad (6)$$

where the observable A averaged over the sample of $i\bar{i}$ candidate events is equal to the raw asymmetry $A_{\text{raw}}^{i\bar{i}}$. By construction, A lies in the interval $[-1, +1]$. For a perfectly reconstructed event without resolution effects, A would be either equal to -1 for $\Delta y_{i\bar{i}} < 0$ or to $+1$ for $\Delta y_{i\bar{i}} > 0$. The use of A allows us to determine the statistical uncertainty on $A_{\text{raw}}^{i\bar{i}}$ as the uncertainty on the average of a distribution.

D. Raw estimate of κP

In the same way as in the previous section, we use the accumulation of the likelihoods $L_z(\cos \theta^+)$ and $L_z(\cos \theta^-)$ to estimate the distributions of $\cos \theta^+$ and $\cos \theta^-$. The distributions $\sum_{\text{events}} L_{z_i}(\cos \theta^+)$ and $\sum_{\text{events}} L_{z_i}(\cos \theta^-)$ are shown in Figs. 3(b) and 3(c), after subtracting the background contributions from the data. The raw asymmetries,

TABLE III. Asymmetry estimates for the $\cos\theta^\pm$ distributions. The raw asymmetry measurement in the data before background subtraction, $A_{\text{raw}}^{\ell^\pm, \text{data}}$, the asymmetry of the background, $A_{\text{raw}}^{\ell^\pm, \text{bkg}}$, and the measurement once the background contribution has been subtracted, $A_{\text{raw}}^{\ell^\pm, \text{data-bkg}}$, are reported. The polarization estimates defined as $\kappa P_{\text{raw}}^{\text{xx}} = A_{\text{raw}}^{\ell^+, \text{xx}} - A_{\text{raw}}^{\ell^-, \text{xx}}$ are also given. All values are reported in percent, together with their statistical uncertainties.

Channel	$A_{\text{raw}}^{\ell^+, \text{data}}$	$A_{\text{raw}}^{\ell^+, \text{bkg}}$	$A_{\text{raw}}^{\ell^+, \text{data-bkg}}$	$A_{\text{raw}}^{\ell^-, \text{data}}$	$A_{\text{raw}}^{\ell^-, \text{bkg}}$	$A_{\text{raw}}^{\ell^-, \text{data-bkg}}$	$\kappa P_{\text{raw}}^{\text{data}}$	$\kappa P_{\text{raw}}^{\text{bkg}}$	$\kappa P_{\text{raw}} = \kappa P_{\text{raw}}^{\text{data-bkg}}$
$e\mu$	5.7 ± 4.1	0.6 ± 2.1	6.2 ± 4.6	-3.3 ± 4.1	2.6 ± 2.1	-4.0 ± 4.6	9.0 ± 5.8	-2.0 ± 2.4	10.2 ± 6.4
ee	13.4 ± 7.2	-3.2 ± 2.0	16.5 ± 8.6	-0.8 ± 7.2	-0.5 ± 2.1	-0.9 ± 8.6	14.2 ± 10.1	-2.7 ± 2.3	17.4 ± 12.0
$\mu\mu$	-9.4 ± 8.1	3.9 ± 3.6	-11.5 ± 9.4	-3.7 ± 8.1	2.3 ± 3.5	-4.7 ± 9.3	-5.7 ± 11.8	1.5 ± 3.7	-6.9 ± 13.7
Dilepton	4.6 ± 3.3	0.2 ± 1.3	5.2 ± 3.7	-2.9 ± 3.3	1.7 ± 1.2	-3.5 ± 3.7	7.5 ± 4.7	-1.5 ± 1.4	8.7 ± 5.3

TABLE IV. Measurement of the statistical correlation between the asymmetry $A_{\text{raw}}^{\tilde{t}\tilde{t}}$ and the polarization κP_{raw} for the data, background, and background-subtracted data. Values are reported in percent, together with their statistical uncertainties.

Channel	Data	Background	Data-Background
$e\mu$	27 ± 6	9 ± 3	28 ± 6
ee	10 ± 12	9 ± 3	9 ± 14
$\mu\mu$	36 ± 10	6 ± 5	39 ± 12
Dilepton	26 ± 5	9 ± 2	28 ± 5

$A_{\text{raw}}^{\ell^+}$ and $A_{\text{raw}}^{\ell^-}$, and the raw polarization $\kappa P_{\text{raw}} = A_{\text{raw}}^{\ell^+} - A_{\text{raw}}^{\ell^-}$ extracted from the data are reported in Table III. As for $A_{\text{raw}}^{\tilde{t}\tilde{t}}$, the measurement of κP_{raw} needs to be calibrated to retrieve the parton-level values of the polarization.

E. Statistical correlation between $A_{\text{raw}}^{\tilde{t}\tilde{t}}$ and κP_{raw}

We measure the statistical correlation between $A_{\text{raw}}^{\tilde{t}\tilde{t}}$ and κP_{raw} in the data, which is needed to determine the statistical correlation between the measurements of $A^{\tilde{t}\tilde{t}}$ and κP . In the same way as $A_{\text{raw}}^{\tilde{t}\tilde{t}}$ is the average of an event-by-event asymmetry A , the raw asymmetries $A_{\text{raw}}^{\ell^+}$ and $A_{\text{raw}}^{\ell^-}$ are the averages of event-by-event asymmetries denoted by $A_{\cos\theta^+}$ and $A_{\cos\theta^-}$. The correlation between $A_{\text{raw}}^{\tilde{t}\tilde{t}}$ and κP_{raw} is identical to the correlation between the observables A and $(A_{\cos\theta^+} - A_{\cos\theta^-})$. This correlation is determined from the background-subtracted data by computing the rms and mean values of the distributions of A , $(A_{\cos\theta^+} - A_{\cos\theta^-})$, and $A \cdot (A_{\cos\theta^+} - A_{\cos\theta^-})$:

$$\text{cor}(A_{\text{raw}}^{\tilde{t}\tilde{t}}, \kappa P_{\text{raw}}) = \frac{\langle A \cdot (A_{\cos\theta^+} - A_{\cos\theta^-}) \rangle - A_{\text{raw}}^{\tilde{t}\tilde{t}} \cdot \kappa P_{\text{raw}}}{\text{rms}(A) \cdot \text{rms}(A_{\cos\theta^+} - A_{\cos\theta^-})}. \quad (7)$$

We report the values measured in data in Table IV.

VI. RESULTS CORRECTED FOR CALIBRATION

The calibration procedure finds a relation between the raw asymmetry and polarization, $(A_{\text{raw}}^{\tilde{t}\tilde{t}}, \kappa P_{\text{raw}})$, obtained

after subtracting the background contributions, and the true asymmetry and polarization $(A^{\tilde{t}\tilde{t}}, \kappa P)$ of $\tilde{t}\tilde{t}$ events. The calibration procedure corrects for dilution effects that arise from the limited acceptance for $\tilde{t}\tilde{t}$ events, the finite resolution of the kinematic reconstruction, and the simplified assumptions used in the matrix element integration (e.g., leading order ME, no $gg \rightarrow \tilde{t}\tilde{t}$ ME, only two jets considered). The relation is inverted to extract a measurement of $A^{\tilde{t}\tilde{t}}$ and κP from the values of $A_{\text{raw}}^{\tilde{t}\tilde{t}}$ and κP_{raw} observed in data.

The nominal calibration is determined using a sample of simulated $\tilde{t}\tilde{t}$ MC@MC dilepton events. The procedure is repeated with the samples from the other generators (see Secs. IVA and IVB) to determine different systematic uncertainties. We normalize the individual ee , $e\mu$, and $\mu\mu$ contributions to have the same proportions as observed in the data samples after subtracting the expected backgrounds.

A. Samples for calibration

We produce test samples from a nominal MC sample by reweighting the events according to the true value of the parton level $\Delta y_{\tilde{t}\tilde{t}}$, $\cos\theta^+$, and $\cos\theta^-$. The reweighting factors are computed as follows.

1. Reweighting of lepton angular distributions

The general expression for the double differential lepton angle distribution is [5]

$$\frac{d^2\sigma}{d\cos\theta^+ d\cos\theta^-} = \frac{1}{2} (1 + \kappa^+ P^+ \cos\theta^+ + \kappa^- P^- \cos\theta^- - C \cos\theta^+ \cos\theta^-), \quad (8)$$

where C is the spin correlation coefficient, which is $\approx 90\%$ in the SM. In the beam basis one has $\kappa P \approx \kappa^+ P^+ \approx -\kappa^- P^-$. We use this relation to reweight a given MC sample to simulate a target polarization of $\kappa P_{\text{test}} = \frac{1}{2}(\kappa^+ P^+ - \kappa^- P^-)$.

2. Reweighting of $\Delta y_{\tilde{t}\tilde{t}}$ distribution

To determine a method of reweighting the $\Delta y_{\tilde{t}\tilde{t}}$ distribution, denoted $\mathcal{D}(\Delta y_{\tilde{t}\tilde{t}})$, we study its shape using the

different $t\bar{t}$ MC samples of Sec. IV at the generated level, i.e., before event selection and reconstruction. Inspired by the studies performed for the distribution of rapidity of the charged leptons in Ref. [56], we rewrite $\mathcal{D}(\Delta y_{t\bar{t}})$ as

$$\mathcal{D}(\Delta y_{t\bar{t}}) = \frac{1}{2} (\mathcal{D}(\Delta y_{t\bar{t}}) + \mathcal{D}(-\Delta y_{t\bar{t}})) \cdot (1 + \mathcal{A}(\Delta y_{t\bar{t}})), \quad (9)$$

where $\mathcal{A}(\Delta y_{t\bar{t}}) = \frac{\mathcal{D}(\Delta y_{t\bar{t}}) - \mathcal{D}(-\Delta y_{t\bar{t}})}{\mathcal{D}(\Delta y_{t\bar{t}}) + \mathcal{D}(-\Delta y_{t\bar{t}})}$ is the ratio between the odd and even part of the $\Delta y_{t\bar{t}}$ distribution, also called differential asymmetry as a function of $\Delta y_{t\bar{t}}$; we then fit $\mathcal{A}(\Delta y_{t\bar{t}})$ with an empirical odd function

$$f(\Delta y_{t\bar{t}}) = \beta \times \tanh\left(\frac{\Delta y_{t\bar{t}}}{\alpha}\right) + \beta \times \left(\frac{\Delta y_{t\bar{t}}}{\gamma}\right)^3, \quad (10)$$

where α and γ are shape parameters, while β is a magnitude parameter. The term $\beta \times \left(\frac{\Delta y_{t\bar{t}}}{\gamma}\right)^3$ was not needed in the study of Ref. [56], but improves the modeling significantly for the case of $\Delta y_{t\bar{t}}$. The results of the fit for different $t\bar{t}$ MC samples are shown in Fig. 4. If we reweight a MC sample so that the even part of the $\Delta y_{t\bar{t}}$ distribution, the term α , and the term γ are preserved, then the forward-backward asymmetry is proportional to β .

These considerations yield the following procedure to produce a sample of test asymmetry $A_{\text{test}}^{t\bar{t}}$ starting from a MC sample of generated asymmetry $A_{\text{sample}}^{t\bar{t}}$. We first fit the differential asymmetry at the generated level $\mathcal{A}(\Delta y_{t\bar{t}})$ with the function f of Eq. (10) and determine the parameters α , β , and γ . Then we apply weights to the events processed through the D0 simulation

$$w(\Delta y_{t\bar{t}}) = \frac{1 + \frac{A_{\text{test}}^{t\bar{t}}}{A_{\text{sample}}^{t\bar{t}}} f(\Delta y_{t\bar{t}})}{1 + f(\Delta y_{t\bar{t}})}. \quad (11)$$

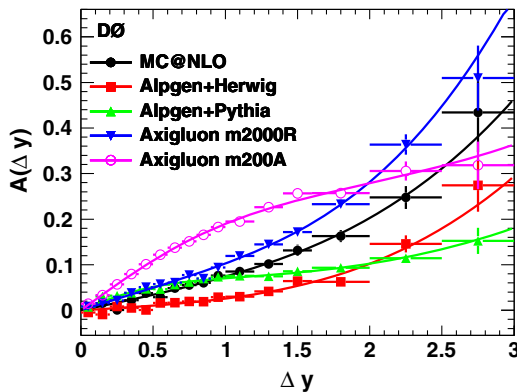


FIG. 4 (color online). Differential asymmetry $\mathcal{A}(\Delta y_{t\bar{t}})$ at parton level for different MC samples. See Ref. [41] for the details on axigluon models. The observed $\mathcal{A}(\Delta y_{t\bar{t}})$ is fitted with the functional form of Eq. (10).

This procedure preserves the even part of the distribution of $\Delta y_{t\bar{t}}$. It also preserves the original shape of the differential asymmetry, but changes its magnitude to the desired value.

3. Calibration

Starting from the nominal MC@NLO $t\bar{t}$ sample, we produce test samples using the product of the weights defined in Secs. VI A 1 and VI A 2. We use a grid of values for polarizations of $\kappa P = (-0.2, -0.1, 0, 0.1, 0.2)$ and asymmetries of $A^{t\bar{t}} = (-0.1, 0, 0.1, 0.15, 0.2, 0.25)$ to obtain 30 samples in addition to the unweighted nominal sample. We apply the method of ME reconstruction to each of the 31 fully simulated samples and extract a raw measurement $(A_{\text{raw}}^{t\bar{t}}, \kappa P_{\text{raw}})$ associated with a given parton level $(A^{t\bar{t}}, \kappa P)$. A fit to the obtained set of points in the space $(A^{t\bar{t}}, \kappa P, A_{\text{raw}}^{t\bar{t}}, \kappa P_{\text{raw}})$ determines two affine functions that relate the reconstructed quantities to the true quantities: $A_{\text{raw}}^{t\bar{t}} = f_1(A^{t\bar{t}}, \kappa P)$ and $\kappa P_{\text{raw}} = f_2(A^{t\bar{t}}, \kappa P)$. The affine functions fit the 31 points well, with residuals $< 0.1\%$. We rewrite the affine relations using a matrix equation:

$$\begin{pmatrix} A_{\text{raw}}^{t\bar{t}} \\ \kappa P_{\text{raw}} \end{pmatrix} = C \cdot \begin{pmatrix} A^{t\bar{t}} \\ \kappa P \end{pmatrix} + O, \quad (12)$$

where C is a 2×2 calibration matrix and O is a vector of offset terms. The values of the matrix C and O are reported in Table V for the different dilepton channels. To determine the statistical uncertainties on the calibration parameters, we use an ensemble method. We split the MC@NLO samples into 100 independent ensembles and then repeat the calibration procedure for each of them.

B. Measurement of $A^{t\bar{t}}$ and κP after calibration

The calibration relation of Eq. (12) is inverted to retrieve the true partonic asymmetry $A^{t\bar{t}}$ and the true polarization κP from the reconstructed $A_{\text{raw}}^{t\bar{t}}$ and κP_{raw} . We obtain a measurement of $(A^{t\bar{t}}, \kappa P)$ reported in Table VI for each dileptonic channel using the calibration coefficients from Table V and the raw measurements from Tables II and III.

TABLE V. Calibration parameters and their statistical uncertainties for the different channels.

Channel	Calibration Matrix C	Offset O
$e\mu$	$\begin{pmatrix} 0.617 \pm 0.008 & 0.148 \pm 0.002 \\ 0.346 \pm 0.008 & 0.560 \pm 0.003 \end{pmatrix}$	$\begin{pmatrix} 0.011 \pm 0.002 \\ -0.009 \pm 0.003 \end{pmatrix}$
ee	$\begin{pmatrix} 0.599 \pm 0.006 & 0.135 \pm 0.003 \\ 0.315 \pm 0.007 & 0.544 \pm 0.005 \end{pmatrix}$	$\begin{pmatrix} 0.007 \pm 0.003 \\ -0.003 \pm 0.005 \end{pmatrix}$
$\mu\mu$	$\begin{pmatrix} 0.639 \pm 0.007 & 0.189 \pm 0.004 \\ 0.460 \pm 0.008 & 0.649 \pm 0.006 \end{pmatrix}$	$\begin{pmatrix} 0.006 \pm 0.005 \\ -0.006 \pm 0.007 \end{pmatrix}$
Dilepton	$\begin{pmatrix} 0.617 \pm 0.008 & 0.153 \pm 0.002 \\ 0.359 \pm 0.006 & 0.572 \pm 0.002 \end{pmatrix}$	$\begin{pmatrix} 0.010 \pm 0.002 \\ -0.007 \pm 0.003 \end{pmatrix}$

TABLE VI. Measurements of $A^{\bar{t}\bar{t}}$ and κP for each dileptonic channel corrected for the calibration (for $m_t = 172.5$ GeV). The statistical correlation between the two measurements arises both from the statistical correlation of the experimental observables and the correction for the calibration.

Channel	$A^{\bar{t}\bar{t}}$ (%)	κP (%)	Statistical Correlation (%)
$e\mu$	$11.6 \pm 7.8(\text{stat})$	$12.6 \pm 13.0(\text{stat})$	-48
ee	$26.1 \pm 15.2(\text{stat})$	$17.5 \pm 26.0(\text{stat})$	-58
$\mu\mu$	$17.8 \pm 16.7(\text{stat})$	$-22.2 \pm 24.6(\text{stat})$	-52
Dilepton	$15.0 \pm 6.4(\text{stat})$	$7.0 \pm 10.5(\text{stat})$	-50

Two ALPGEN+PYTHIA $\bar{t}\bar{t}$ samples generated at different m_t are used to estimate the dependence of the measurement on m_t . Considering a top mass of $m_t = 173.18 \pm 0.94$ GeV [40] as reference, the dilepton results reported in Table VI have to be corrected by -0.02% and 0.15% for $A^{\bar{t}\bar{t}}$ and κP , respectively. The corrected combined dilepton results are

$$A^{\bar{t}\bar{t}} = (15.0 \pm 6.4 (\text{stat}))\% \quad (13)$$

$$\kappa P = (7.2 \pm 10.5 (\text{stat}))\%. \quad (14)$$

VII. SYSTEMATIC UNCERTAINTIES

We consider three categories of uncertainties. Uncertainties affecting the signal are obtained by deriving calibration coefficients from alternate signal models and propagating them to the final results. Uncertainties affecting the background have an impact on the raw measurements, $A_{\text{raw}}^{\bar{t}\bar{t}}$ and κP_{raw} , as these observables are obtained after subtracting the background. They are propagated to the final measurement by applying the nominal calibration correction to the modified $A_{\text{raw}}^{\bar{t}\bar{t}}$ and κP_{raw} . The third category consists of the uncertainties on the calibration method. Since the measurement is performed after background subtraction, the calibration is independent of the normalization of the $\bar{t}\bar{t}$ simulation, and there is no systematic uncertainty due to signal normalization. The uncertainties on $A^{\bar{t}\bar{t}}$ and κP due to the different sources are summarized in Table VII, together with the correlations.

A. Uncertainties on signal

Several sources of systematic uncertainties due to the detector and reconstruction model affect the jets and thus the signal kinematics. We consider uncertainties on the jet energy scale, flavor-dependent jet response, and jet energy resolution [32]. We also take into account uncertainties associated with b tagging and vertexing [34].

To estimate the impact of higher order correction, we compare the calibration obtained with MC@NLO+HERWIG to the calibration obtained with ALPGEN+HERWIG. To propagate uncertainty on the simulation of initial state and final state radiations (ISR/FSR), the amount of radiation is

TABLE VII. Summary of systematic and statistical uncertainties.

Source of Uncertainty	Uncertainty on $A^{\bar{t}\bar{t}}$ (%)	Uncertainty on κP (%)	Correlation (%)
<i>Detector modeling</i>			
Jet energy scale	0.13	0.50	-100
Jet energy resolution	0.03	0.06	100
Flavor-dependent jet response	0.02	0.06	-100
b tagging	0.14	0.43	-94
<i>Signal modeling</i>			
ISR/FSR	0.16	0.41	-100
Forward/backward ISR	0.10	0.07	-100
Hadronization and showering	3.28	1.94	-100
Higher order correction	0.02	0.71	-100
PDF	0.12	0.30	-98
Top-quark mass	0.03	0.21	-100
<i>Background model</i>			
Instrumental background shape	0.16	0.53	100
Instrumental background normalization	0.29	0.01	100
Background normalization	0.44	0.18	100
<i>Calibration</i>			
$\Delta y_{\bar{t}\bar{t}}$ model	1.28	0.11	100
MC statistics	0.60	0.61	-39
<i>Model dependence</i>			
Maximum $A^{\bar{t}\bar{t}}$ variation	2.91	2.35	-100
Maximum κP variation	1.49	2.58	-100
<i>Statistical uncertainty</i>			
Total systematic without model dependence	3.62	2.40	-74
Total systematic	4.88	4.24	-83
Total	8.05	11.35	-56

varied by scaling the ktfac parameter either by a factor of 1.5 or $1/1.5$ in an ALPGEN+PYTHIA simulation of $\bar{t}\bar{t}$ events [50]. The hadronization and parton-shower model uncertainty is derived from the difference between the PYTHIA and HERWIG generators, estimated by comparing ALPGEN+HERWIG to ALPGEN+PYTHIA $\bar{t}\bar{t}$ samples. The different models for parton showers used by various MC generators yield different amounts of ISR between forward and backward events [57,58]. The uncertainty on the ISR model is defined as 50% of the difference between the nominal results and the results derived from a MC@NLO simulation in which the dependence of the forward-backward asymmetry on the p_T of the $\bar{t}\bar{t}$ system is removed. The uncertainty of 0.94 GeV on m_t [40] is propagated to the final result using two ALPGEN+PYTHIA samples generated

with different m_t values. We determine PDF uncertainties by varying the 20 parameters describing the CTEQ6M1 PDF [35] within their uncertainties.

B. Uncertainties on background

The uncertainty on the background level is obtained by varying the instrumental background normalization by 50% and the overall background normalization by 20%. The model of the instrumental background kinematics is varied, using the same method as in Ref. [15]. We reweight the reconstructed Δy , $\cos\theta^+$, and $\cos\theta^-$ distributions by a factor of $1 + \epsilon \times \sigma_{\text{band}}$, where σ_{band} is the statistical uncertainty band of the distribution and $\epsilon = \pm 1$ is chosen to be positive for $\Delta y > 0$, $\cos\theta^+ > 0$, $\cos\theta^- < 0$, and negative for $\Delta y < 0$, $\cos\theta^+ < 0$, and $\cos\theta^- > 0$.

C. Uncertainties on calibration

We also consider sources of uncertainties affecting the calibration procedure. The statistical uncertainty on the calibration parameters and their correlations are propagated to the final measurements. The uncertainties are 0.60% for $A^{\bar{t}}$ and 0.61% for κP . The correlation is -39% .

To estimate a systematic uncertainty due to the choice of $\Delta y_{\bar{t}}$ calibration procedure, we reweight the MC@NLO sample to reproduce the shape of the differential asymmetries of each different BSM and SM model considered. Each of the resulting samples serves as a seed for a new calibration procedure as described in Sec. VI A 2. The maximum variation in the $A^{\bar{t}}$ measurement obtained with these new calibrations is taken as systematic uncertainty. It is obtained using the shape from the ALPGEN+PYTHIA sample and amounts to 1.3%. The impact of these tests is negligible for κP since only the $\Delta y_{\bar{t}}$ distribution is modified.

We also perform a closure test using the five different BSM models described in Sec. IV B. For each of the considered BSM models we create test samples by reweighting the $\Delta y_{\bar{t}}$ and $\cos\theta^\pm$ distributions, in the same way as described in Sec. VI A for MC@NLO samples. The samples cover a range of values of $A^{\bar{t}}$ and κP centered around the data measurement within ± 1 statistical standard deviations. These samples are treated as pseudodata: We compute the differences between what would be measured using the nominal calibration and the true $A^{\bar{t}}$ and κP of each sample. The maximum $A^{\bar{t}}$ bias is found for the axigluon $m200L$ sample [41] and corresponds to a shift of $(\Delta A^{\bar{t}}, \Delta \kappa P) = (-2.9\%, 2.3\%)$ obtained for $(A^{\bar{t}}, \kappa P) \approx (19\%, 9\%)$. The maximum κP bias is found for the axigluon $m200A$ sample [41] and corresponds to $(\Delta A^{\bar{t}}, \Delta \kappa P) = (-1.5\%, 2.6\%)$ for $(A^{\bar{t}}, \kappa P) \approx (10\%, 0\%)$. These two doublets in $(\Delta A^{\bar{t}}, \Delta \kappa P)$ are taken as uncorrelated systematic uncertainties. In each of these doublets, the uncertainty on $A^{\bar{t}}$ and κP are taken as -100% correlated.

VIII. RESULTS

The measurements and the uncertainties discussed in the previous sections are summarized by

$$\begin{aligned} A^{\bar{t}} &= (15.0 \pm 6.4 \text{ (stat)} \pm 4.9 \text{ (syst)})\%, \\ \kappa P &= (7.2 \pm 10.5 \text{ (stat)} \pm 4.2 \text{ (syst)})\%, \end{aligned} \quad (15)$$

with a correlation of -56% between the measurements. The results are presented in Fig. 5. The NLO SM prediction for $A^{\bar{t}}$ is $A^{\bar{t}} = (9.5 \pm 0.7)\%$ [2], while the SM polarization is expected to be small, $\kappa P = (-0.19 \pm 0.05)\%$ [4]. Our measurement is consistent with the SM prediction within the 68% confidence level region. In Fig. 5 we overlay the expected values for the different axigluon models of Ref. [41]. As the models are generated with the LO MadGraph generator, we add an asymmetry of 9.5% arising from the pure SM contributions that is not accounted for by MadGraph. The approximation of just adding the MadGraph LO asymmetry to the SM asymmetry is estimated to be valid at the $\approx 3\%$ level.

We interpret the measurements as a test of the SM, separately assuming the SM forward-backward asymmetry of $A^{\bar{t}} = (9.5 \pm 0.7)\%$ and the SM polarization of $\kappa P = (-0.19 \pm 0.05)\%$. As we assume the SM, we do not consider the uncertainty from the dependence on the physics model. The constraint on $A^{\bar{t}}$ is applied to the two-dimensional result of Eq. (15) to obtain the polarization

$$\kappa P = (11.3 \pm 9.1 \text{ (stat)} \pm 1.9 \text{ (syst)})\%. \quad (16)$$

This result is consistent with the SM expectation at the 1.2 standard deviation level. Applying the constraint on κP we obtain an asymmetry of

$$A^{\bar{t}} = (17.5 \pm 5.6 \text{ (stat)} \pm 3.1 \text{ (syst)})\%, \quad (17)$$

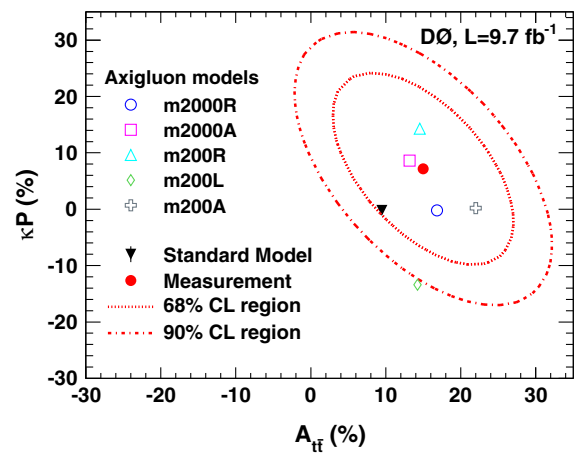


FIG. 5 (color online). Two-dimensional visualization of the $A^{\bar{t}}$ and κP measurements and comparison with benchmark axigluon models [41].

which is consistent with the SM expectation at the 1.3 standard deviation level.

In a previous publication, the D0 Collaboration has measured the forward-backward asymmetry in the lepton + jets channel [11]:

$$A^{\bar{t}t} = (10.6 \pm 2.8 \text{ (stat)} \pm 1.3 \text{ (syst)})\% = (10.6 \pm 3.0)\%. \quad (18)$$

This lepton + jets measurement was performed in the context of a test of the SM, as no study of the dependence with respect to the possible polarization was performed. Therefore, it should be compared with the result of Eq. (17). We classify the systematic uncertainties of both measurements by their sources and consider them as being either completely correlated, e.g., the b -tagging uncertainty, or completely uncorrelated, e.g., the background modeling. Even if some sources of uncertainties are correlated between both channels, the dominant sources are not, so that the final overall uncertainties are only 7% correlated. The two measurements are consistent with a probability of 30% given by a χ^2 test. We combine the lepton + jets and dilepton measurements, using the best linear unbiased estimate [59,60]. The combination is a weighted average of the input measurements, with the dilepton measurement given a weight of 0.17 and the lepton + jets measurement a weight of 0.83. The combined result is

$$A^{\bar{t}t} = 11.8 \pm 2.5 \text{ (stat)} \pm 1.3 \text{ (syst)}\%. \quad (19)$$

IX. SUMMARY

We have presented a simultaneous measurement of the forward-backward asymmetry of $\bar{t}t$ production and the top-quark spin polarization in the beam basis in dilepton final states, using 9.7 fb^{-1} of proton-antiproton collisions at $\sqrt{s} = 1.96 \text{ TeV}$ with the D0 detector. The results are

$$\begin{aligned} A^{\bar{t}t} &= (15.0 \pm 8.0)\%, \\ \kappa P &= (7.2 \pm 11.3)\%, \end{aligned} \quad (20)$$

with a correlation of -56% between the measurements. They are consistent with the SM expectations within the 68% confidence level region.

Interpreted as a test of the SM and assuming the SM forward-backward asymmetry, these results yield a measurement of the top polarization of

$$\kappa P = (11.3 \pm 9.3)\%. \quad (21)$$

Assuming the SM polarization, we obtain a forward-backward asymmetry of

$$A^{\bar{t}t} = (17.5 \pm 6.3)\%. \quad (22)$$

This asymmetry is combined with the measurement of the asymmetry in lepton + jets final states yielding a combined asymmetry of

$$A^{\bar{t}t} = (11.8 \pm 2.8)\%. \quad (23)$$

All of these results are consistent with the SM expectations within uncertainties.

ACKNOWLEDGMENTS

We thank the staffs at Fermilab and collaborating institutions, and acknowledge support from the Department of Energy and National Science Foundation (U.S.); Alternative Energies and Atomic Energy Commission and National Center for Scientific Research/National Institute of Nuclear and Particle Physics (France); Ministry of Education and Science of the Russian Federation, National Research Center “Kurchatov Institute” of the Russian Federation, and Russian Foundation for Basic Research (Russia); National Council for the Development of Science and Technology and Carlos Chagas Filho Foundation for the Support of Research in the State of Rio de Janeiro (Brazil); Department of Atomic Energy and Department of Science and Technology (India); Administrative Department of Science, Technology and Innovation (Colombia); National Council of Science and Technology (Mexico); National Research Foundation of Korea (Korea); Foundation for Fundamental Research on Matter (The Netherlands); Science and Technology Facilities Council and The Royal Society (United Kingdom); Ministry of Education, Youth and Sports (Czech Republic); Bundesministerium für Bildung und Forschung (Federal Ministry of Education and Research) and Deutsche Forschungsgemeinschaft (German Research Foundation) (Germany); Science Foundation Ireland (Ireland); Swedish Research Council (Sweden); China Academy of Sciences and National Natural Science Foundation of China (China); and Ministry of Education and Science of Ukraine (Ukraine).

- [1] W. Bernreuther and Z.-G. Si, Top quark and leptonic charge asymmetries for the Tevatron and LHC, *Phys. Rev. D* **86**, 034026 (2012).
- [2] M. Czakon, P. Fiedler, and A. Mitov, Resolving the Tevatron Top Quark Forward-Backward Asymmetry Puzzle: Fully Differential Next-to-Next-to-Leading-Order Calculation, *Phys. Rev. Lett.* **115**, 052001 (2015).
- [3] N. Kidonakis, The top quark forward-backward asymmetry at approximate N³LO, *Phys. Rev. D* **91**, 071502 (2015).
- [4] W. Bernreuther, M. Fuecker, and Z.-G. Si, Weak interaction corrections to hadronic top quark pair production, *Phys. Rev. D* **74**, 113005 (2006); (private communication).
- [5] W. Bernreuther, Top quark physics at the LHC, *J. Phys. G* **35**, 083001 (2008).
- [6] P. H. Frampton and S. L. Glashow, Chiral color: An alternative to the standard model, *Phys. Lett. B* **190**, 157 (1987).
- [7] L. J. Hall and A. E. Nelson, Heavy gluons and monojets, *Phys. Lett.* **153B**, 430 (1985).
- [8] O. Antunano, J. H. Kühn, and G. Rodrigo, Top quarks, axigluons, and charge asymmetries at hadron colliders, *Phys. Rev. D* **77**, 014003 (2008).
- [9] P. H. Frampton, J. Shu, and K. Wang, Axigluon as possible explanation for $p\bar{p} \rightarrow t\bar{t}$ forward-backward asymmetry, *Phys. Lett. B* **683**, 294 (2010).
- [10] T. Aaltonen *et al.* (CDF Collaboration), Measurement of the top quark forward-backward production asymmetry and its dependence on event kinematic properties, *Phys. Rev. D* **87**, 092002 (2013).
- [11] V. M. Abazov *et al.* (D0 Collaboration), Measurement of the forward-backward asymmetry in top quark-antiquark production in $p\bar{p}$ collisions using the lepton + jets channel, *Phys. Rev. D* **90**, 072011 (2014).
- [12] T. Aaltonen *et al.* (CDF Collaboration), Measurement of the leptonic asymmetry in $t\bar{t}$ events produced in $p\bar{p}$ collisions at $\sqrt{s} = 1.96$ TeV, *Phys. Rev. D* **88**, 072003 (2013).
- [13] T. Aaltonen *et al.* (CDF Collaboration), Measurement of the Inclusive Leptonic Asymmetry in Top-Quark Pairs that Decay to Two Charged Leptons at CDF, *Phys. Rev. Lett.* **113**, 042001 (2014).
- [14] V. M. Abazov *et al.* (D0 Collaboration), Measurement of the forward-backward asymmetry in the distribution of leptons in $t\bar{t}$ events in the lepton + jets channel, *Phys. Rev. D* **90**, 072001 (2014).
- [15] V. M. Abazov *et al.* (D0 Collaboration), Measurement of the asymmetric in angular distributions of leptons produced in dilepton $t\bar{t}$ final states in $p\bar{p}$ collisions at $\sqrt{s} = 1.96$ TeV, *Phys. Rev. D* **88**, 112002 (2013).
- [16] J. A. Aguilar-Saavedra, D. Amidei, A. Juste, and M. Perez-Victoria, Asymmetries in top quark pair production at hadron colliders, *Rev. Mod. Phys.* **87**, 421 (2015).
- [17] V. M. Abazov *et al.* (D0 Collaboration), Measurement of leptonic asymmetries and top quark polarization in $t\bar{t}$ production, *Phys. Rev. D* **87**, 011103 (2013).
- [18] S. Chatrchyan *et al.* (CMS Collaboration), Measurements of $t\bar{t}$ Spin Correlations and Top-Quark Polarization Using Dilepton Final States in pp Collisions at $\sqrt{s} = 7$ TeV, *Phys. Rev. Lett.* **112**, 182001 (2014).
- [19] G. Aad *et al.* (ATLAS Collaboration), Measurement of Top Quark Polarization in Top-Antitop Events from Proton-Proton Collisions at $\sqrt{s} = 7$ TeV Using the ATLAS Detector, *Phys. Rev. Lett.* **111**, 232002 (2013).
- [20] V. M. Abazov *et al.* (D0 Collaboration), Precise Measurement of the Top Quark Mass in the Dilepton Channel at D0, *Phys. Rev. Lett.* **107**, 082004 (2011).
- [21] S. Frixione and B. R. Webber, Matching NLO QCD computations and parton shower simulations, *J. High Energy Phys.* **06** (2002) 029.
- [22] S. Frixione and B. R. Webber, The MC@NLO 3.4 event generator, arXiv:0812.0770.
- [23] S. Abachi *et al.* (D0 Collaboration), The D0 detector, *Nucl. Instrum. Methods Phys. Res., Sect. A* **338**, 185 (1994).
- [24] V. M. Abazov *et al.* (D0 Collaboration), The upgraded D0 detector, *Nucl. Instrum. Methods Phys. Res., Sect. A* **565**, 463 (2006).
- [25] M. Abolins *et al.*, Design and implementation of the new D0 level-1 calorimeter trigger, *Nucl. Instrum. Methods Phys. Res., Sect. A* **584**, 75 (2008).
- [26] R. Angstadt *et al.* (D0 Collaboration), The layer 0 inner silicon detector of the D0 experiment, *Nucl. Instrum. Methods Phys. Res., Sect. A* **622**, 298 (2010).
- [27] The pseudorapidity is defined as $\eta = -\ln(\tan\theta/2)$, where θ is the polar angle relative to the proton beam direction.
- [28] V. M. Abazov *et al.* (D0 Collaboration), Electron and photon identification in the D0 experiment, *Nucl. Instrum. Methods Phys. Res., Sect. A* **750**, 78 (2014).
- [29] V. M. Abazov *et al.* (D0 Collaboration), Muon reconstruction and identification with the Run II D0 detector, *Nucl. Instrum. Methods Phys. Res., Sect. A* **737**, 281 (2014).
- [30] G. C. Blazey *et al.*, Run II jet physics, arXiv:hep-ex/0005012.
- [31] Here, $\mathcal{R} = \sqrt{(\Delta\phi)^2 + (\Delta\eta)^2}$, where ϕ is the azimuthal angle around the proton beam direction.
- [32] V. M. Abazov *et al.* (D0 Collaboration), Jet energy scale determination in the D0 experiment, *Nucl. Instrum. Methods Phys. Res., Sect. A* **763**, 442 (2014).
- [33] A. Schwartzman, Ph.D. thesis, University of Buenos Aires, 2004 [Fermilab-Thesis-2004-21].
- [34] V. M. Abazov *et al.* (D0 Collaboration), Improved b quark jet identification at the D0 experiment, *Nucl. Instrum. Methods Phys. Res., Sect. A* **763**, 290 (2014).
- [35] P. M. Nadolsky, Hung-Liang Lai, Qing-Hong Cao, Joey Huston, Jon Pumplin, Daniel Stump, Wu-Ki Tung, and C.-P. Yuan, Implications of CTEQ global analysis for collider observables, *Phys. Rev. D* **78**, 013004 (2008).
- [36] G. Corcella, I. G. Knowles, G. Marchesini, S. Moretti, K. Odagiri, P. Richardson, M. H. Seymour, and B. R. Webber, HERWIG 6.5: An event generator for hadron emission reactions with interfering gluons (including supersymmetric processes), *J. High Energy Phys.* **01** (2001) 010.
- [37] M. L. Mangano, F. Piccinini, A. D. Polosa, M. Moretti, and R. Pittau, ALPGEN, a generator for hard multiparton processes in hadronic collisions, *J. High Energy Phys.* **07** (2003) 001.
- [38] T. Sjostrand, S. Mrenna, and P. Z. Skands, PYTHIA 6.4 physics and manual, *J. High Energy Phys.* **05** (2006) 026.
- [39] S. Moch and P. Uwer, Theoretical status and prospects for top-quark pair production at hadron colliders, *Phys. Rev. D* **78**, 034003 (2008).

- [40] T. Aaltonen *et al.* (CDF and D0 Collaborations), Combination of the top-quark mass measurements from the Tevatron collider, *Phys. Rev. D* **86**, 092003 (2012).
- [41] A. Carmona, M. Chala, A. Falkowski, S. Khatibi, M. M. Najafabadi, G. Perez, and J. Santiago, From Tevatron's top and lepton-based asymmetries to the LHC, *J. High Energy Phys.* **07** (2014) 005.
- [42] J. Alwall, R. Frederix, S. Frixione, V. Hirschi, F. Maltoni, O. Mattelaer, H.-S. Shao, T. Stelzer, P. Torrielli, and M. Zaro, The automated computation of tree-level and next-to-leading order differential cross sections, and their matching to parton shower simulations, *J. High Energy Phys.* **07** (2014) 079.
- [43] V. M. Abazov *et al.* (D0 Collaboration), Measurement of differential $t\bar{t}$ production cross sections in $p\bar{p}$ collisions, *Phys. Rev. D* **90**, 092006 (2014).
- [44] R. Gavin, Y. Li, F. Petriello, and S. Quackenbush, FEWZ 2.0: A code for hadronic Z production at next-to-next-to-leading order, *Comput. Phys. Commun.* **182**, 2388 (2011).
- [45] V. Abazov *et al.* (D0 Collaboration), Measurement of the Shape of the Boson Transverse Momentum Distribution in $p\bar{p} \rightarrow Z/\gamma^* \rightarrow e^+e^- + X$ Events Produced at $\sqrt{s} = 1.96$ TeV, *Phys. Rev. Lett.* **100**, 102002 (2008).
- [46] J. M. Campbell and R. K. Ellis, An update on vector boson pair production at hadron colliders, *Phys. Rev. D* **60**, 113006 (1999).
- [47] J. M. Campbell and R. K. Ellis, MCFM for the Tevatron and the LHC, *Nucl. Phys. B, Proc. Suppl.* **205–206**, 10 (2010).
- [48] R. Brun and F. Carminati, CERN program library long writeup W5013 (unpublished).
- [49] V. Abazov *et al.* (D0 Collaboration), Measurement of the $t\bar{t}$ production cross section in $p\bar{p}$ collisions at $\sqrt{s} = 1.96$ TeV using kinematic characteristics of lepton + jets events, *Phys. Rev. D* **76**, 092007 (2007).
- [50] V. M. Abazov *et al.* (D0 Collaboration), Precision measurement of the top-quark mass in lepton + jets final states, *Phys. Rev. D* **91**, 112003 (2015).
- [51] A. Grohsjean, Ph.D. thesis, Munich University, 2008 [Fermilab-Thesis-2008-92].
- [52] K. A. Olive *et al.* (Particle Data Group), Review of particle physics, *Chin. Phys. C* **38**, 090001 (2014).
- [53] G. Lepage, A new algorithm for adaptive multidimensional integration, *J. Comp. Phys.* **27**, 192 (1978).
- [54] G. Lepage, Report No. CLNS:80-447, 1980.
- [55] M. Galassi *et al.*, *GNU Scientific Library Reference Manual* (Network Theory Ltd., United Kingdom, 2009), 3rd ed., <http://www.gnu.org/software/gsl/>.
- [56] Z. Hong, R. Edgar, S. Henry, D. Toback, J. S. Wilson, D. Amidei, On the forward-backward asymmetry of leptonic decays of $t\bar{t}$ at the Fermilab Tevatron, *Phys. Rev. D* **90**, 014040 (2014).
- [57] P. Skands, B. Webber, and J. Winter, QCD coherence and the top quark asymmetry, *J. High Energy Phys.* **07** (2012) 151.
- [58] J. Winter, P. Z. Skands, and B. R. Webber, Monte Carlo event generators and the top quark forward-backward asymmetry, *EPJ Web Conf.* **49**, 17001 (2013).
- [59] L. Lyons, D. Gibaut, and P. Clifford, How to combine correlated estimates of a single physical quantity, *Nucl. Instrum. Methods Phys. Res., Sect. A* **270**, 110 (1988).
- [60] A. Valassi, Combining correlated measurements of several different physical quantities, *Nucl. Instrum. Methods Phys. Res., Sect. A* **500**, 391 (2003).